JOURNAL OF THERMOPHYSICS AND HEAT TRANSFER
Vol. 8, No. 4, Oct.–Dec. 1994

Adaptive Remeshing for Convective Heat Transfer with Variable Fluid Properties

Dominique Pelletier,* Florin Ilinca,† and Jean-François Hétu‡
École Polytechnique de Montréal, Montréal, Québec H3C 3A7, Canada

This article presents an adaptive finite element method based on remeshing to solve incompressible viscous flow problems for which fluid properties present a strong temperature dependence. Solutions are obtained in primitive variables using a highly accurate finite element approximation on unstructured grids. Two general purpose error estimators are presented, which take into account the temperature dependence of fluid properties. The methodology is applied to a problem of practical interest: the thermal convection of corn syrup in an enclosure with localized heating. Predictions are in good agreement with experimental measurements. The method leads to improved accuracy and reliability of finite element predictions.

Nomenclature

c_p = specific heat
e = error
$\boldsymbol{g}$ = gravity vector
h = element size
k = thermal conductivity
$\boldsymbol{n}$ = outward unit vector
Pr = Prandtl number
p = pressure
$\boldsymbol{q}$ = heat flux vector
Ra = Rayleigh number
T = temperature
$\boldsymbol{u}$ = velocity vector
v, s, w = test functions
β = volume expansion coefficient
δ = element size for new mesh
η = relative error
μ = viscosity
ρ = density
τ = stress tensor

Subscripts
av = average
h = finite element solution
0 = reference value
∂, B = boundary

Introduction

MOST real life computational fluid dynamics (CFD) simulations of concern are characterized by the extreme nature of the geometry or values of the flow parameters: high aspect ratios, high Reynolds numbers for isothermal problems, or high Rayleigh numbers for free convection. Problems vary greatly in their respective placement in fluid flow parameters: turbulent flows are characterized by large spatial variations of the effective viscosity; thermal processing of oils and other foods are characterized by a strong nonlinear dependence of fluid properties on temperature (viscosity may vary by as much as three orders of magnitude). Finally, materials having vastly different physical properties are often juxtaposed, leading to the appearance of quasisingularities.

Such problems place special demands on the solution algorithm. The technique must be robust and provide solutions for a wide range of parameters. Furthermore, in many cases it is difficult to determine a priori where the mesh must be refined in order to accurately capture the physics of the problems. This article presents an adaptive finite element method capable of tackling these difficulties.

Adaptive finite element methods provide a powerful approach for tackling such complex CFD problems because grid points can be automatically clustered in regions of rapid solution variation to improve accuracy. Furthermore, the adaptive process is cost effective in the sense that the best numerical solution is often obtained at the least computational cost. Such approaches thus provide flexibility in modeling and algorithm development and can, at least in theory, provide quantitative measures of the accuracy of the solutions computed. The ability of the methodology to produce uniformly accurate solutions makes it possible to obtain "numerically exact solutions" (grid independent) to the equations of motion, so that mathematical models of the physical phenomenon of interest can be evaluated with confidence.

Initial breakthroughs in adaptive methods were achieved in aerodynamics because of the pressing need for accurate computations of shock waves.[1] However, little work has been done for incompressible flows, and even less for convective heat transfer problems. Proof of concept computations were reported in Refs. 2 and 3. In Refs. 4–8 the methodology proposed by the authors was quantitatively validated by solving flows with known analytical solution and by computing cases for which experimental measurements were available. Cases treated covered isothermal laminar flows, heat transfer by free convection, conjugate heat transfer, and turbulent free shear flows. This article presents a rigorous extension of the authors' methodology to heat transfer problems with variable fluid properties. Taking into account the thermal dependence of the fluid properties is critical to successful predictions in such diverse applications as flows of oils and fuels,[9] food processing, thermal convection in the Earth mantle,[10–12] meteorology, and astrophysics, to name a few.

Chu and Hickox[12] have presented very interesting experimental and computational results for the convection of corn syrup in a cavity with localized heating from below as a means of studying the correlation between convection in the mantle and the movement of tectonic plates. Their experimental study

Received May 26, 1993; presented as Paper 93-2767 at the AIAA 28th Thermophysics Conference, Orlando, FL, July 6–9, 1993; revision received April 29, 1994; accepted for publication May 2, 1994.

*Associate Professor, Mechanical Engineering Department. Member AIAA.
†Graduate Research Assistant, Mechanical Engineering Department.
‡Research Officer; currently at National Research Council of Canada, Institute for Industrial Materials, 75, Montarville, Boucherville, Canada.

included cases for which the viscosity varied by as much as three orders of magnitude. Under these conditions creeping flow exists in some regions of the domain, whereas a highly convective regime is found elsewhere. It is the simultaneous presence of such extremes in flow regimes that motivates the present study.

This article is organized as follows: first the equations of motion and the nonlinear finite element solver are reviewed. The methodology section describes two error estimators and the adaptive remeshing strategy. The method is then applied to thermal convection in an enclosure with localized heating from below for which experimental data are available. This article closes with conclusions.

Modeling of the Problem

Equations of Motion

The flow is modeled by the Navier-Stokes, continuity, and energy equations with the Boussinesq approximation

$$\rho \boldsymbol{u}\cdot\nabla\boldsymbol{u} = -\nabla p + \nabla\cdot\tau + \rho g\beta(T - T_0)$$

$$\nabla\cdot\boldsymbol{u} = 0$$

$$\rho c_p \boldsymbol{u}\cdot\nabla T = \nabla\cdot\boldsymbol{q}$$

where τ is defined by $\tau = \mu[\nabla u + (\nabla u)^T]$, and $\boldsymbol{q} = k\nabla T$ is the heat flux and μ, c_p, and k are all functions of temperature. Appropriate boundary conditions complete the statement of the problem.

Finite Element Solver

The variational equations solved by the finite element method are obtained by multiplying the above equations by appropriate test functions and integrating over the domain of interest. Application of the divergence theorem to the momentum and temperature diffusion terms leads to the following weak form:

$$(\rho u\cdot\nabla u, v) + a(u, v) - (p, \nabla\cdot v) - (\rho g\beta T, v) = -(\rho g\beta T_0, v) + \langle \hat{t}, v\rangle$$

$$(s, \nabla\cdot u) = 0$$

$$(\rho c_p u\cdot\nabla T, w) + d(T, w) = \langle q_B, w\rangle$$

where

$$(f, g) = \int_\Omega fg \, d\Omega$$

$$a(u, v) = \int_\Omega \tau(u):\nabla v \, d\Omega$$

$$d(T, w) = \int_\Omega q(T)\cdot\nabla w \, d\Omega$$

and the boundary terms are given by

$$\langle \hat{t}, v\rangle = \int_{\partial K\cap\Gamma_t} (\tau\cdot n - pn)\cdot v \, ds + \int_{\partial K\cap\Gamma_t} \hat{t}\cdot v \, ds$$

$$\langle q_B, w\rangle = \int_{\partial K\cap\Gamma_q} q\cdot n w \, ds + \int_{\partial K\cap\Gamma_q} q_B w \, ds$$

These variational equations are solved by a standard Galerkin method using the seven-node triangular element that uses an enriched quadratic velocity field, a quadratic temperature, and a linear discontinuous pressure approximation.[4,7] An augmented Lagrangian algorithm is used to treat the incompressibility.[13] Finally, the temperature dependence of the viscosity, specific heat, and conductivity introduces strong nonlinearities that are treated with Newton's method.

Adaptive Methodology

The basic idea behind adaptive methods is to assess the quality of an initial solution obtained on a coarse mesh by using some form of error estimation, and to modify the mesh in a systematic fashion so as to improve the overall quality of the solution. In this work adaptive remeshing has been retained because it provides control of element size and grading to accurately resolve flow features such as shear and thermal layers. In this method the problem is first solved on a coarse grid to roughly capture the physics of the flow. The resulting solution is then analyzed to determine where more grid points are needed, and an improved mesh is generated. The problem is solved again on the new mesh using the solution obtained on the coarser mesh as an initial guess. This process is repeated until the required level of accuracy is achieved. Note that alternative adaptive methods could also be used.[1,3,4,14,15] Remeshing also offers an elegant and simple approach to use the best proven finite element approximations in an adaptive context.[13,16]

Error Estimation

Projection Error Estimator

This technique was first introduced in Ref. 17 and is based on the observation that the derivatives (stresses, heat flux) of the finite element solution are discontinuous across element faces while the exact derivatives are continuous. The difference between the two is a measure of accuracy of the numerical solution. However, the exact solution is not known in cases of practical interest, but an approximation to the true derivatives can be obtained by a least-squares projection of the finite element derivatives:

$$\sum_{K\in T}\left[\int_K \phi_m(\tau_{ij} - \tilde{\tau}_{ij}) \, dx\right] = 0$$

where

$$\tilde{\tau}_{ij} = \sum_{i=1}^{7} \phi_n(\tilde{\tau}_{ij})_n$$

is the projection of the finite element (FEM) stresses τ into the space of the velocity interpolation functions.

This least-squares projection approach is also used to obtain a continuous approximation for the pressure and heat fluxes. The velocity, pressure, and temperature contributions to the error are then given by

$$e^u = \tilde{\boldsymbol{\tau}} - \boldsymbol{\tau}$$

$$e^p = \tilde{p} - p$$

$$e^T = \tilde{\boldsymbol{q}} - \boldsymbol{q}$$

where the "~" denotes the result from the least-squares projection.

The combined norm of the velocity, pressure, and temperature fields and their errors are computed using the following expressions:

$$\|(u, p, T)\| = \{\|\boldsymbol{u}\|_E^2 + \|p\|_0^2 + \|T\|^2\}^{1/2}$$

$$\|(e^u, e^p, e^T)\| = \{\|e^u\|_E^2 + \|e^p\|_0^2 + \|e^T\|^2\}^{1/2}$$

where the individual norms are defined as

$$\|u\|_E^2 = \int_\Omega \boldsymbol{\tau}:\boldsymbol{\tau}\, d\Omega, \qquad \|e^u\|_E^2 = \int_\Omega e^u:e^u\, d\Omega$$

$$\|p\|_0^2 = \int_\Omega |p|^2\, d\Omega, \qquad \|e^p\|_0^2 = \int_\Omega |e^p|^2\, d\Omega$$

$$\|T\| = \int_\Omega \boldsymbol{q}\cdot\boldsymbol{q}\, d\Omega, \qquad \|e^T\|^2 = \int_\Omega e^T\cdot e^T\, d\Omega$$

This is the so-called natural norm induced by the variational formulation of the problem, which includes variations of the fluid properties. This ensures that mesh refinement will occur in regions where the heat flux and shear stress variations are significant. It will avoid over-refinement in cases where temperature and velocity may have steep gradient, but fluid properties that are small enough that the heat flux and stress show little variation.

It should be noted that in the present approach fluxes are projected rather than derivatives, as is suggested in Ref. 17. This approach ensures that the error estimator is well-behaved in cases where physical properties are different in adjacent regions of the domain. The conjugate heat transfer case treated here involves heat conduction through copper and Plexiglas® that have conductivities that differ by several orders of magnitude.

Local Variational Problem for the Error

This approach provides an estimate of the error without having to solve the global least-squares problems required by the previous estimator. Variational equations for the velocity, pressure, and temperature errors can be derived directly from the Navier-Stokes equations[5,18–20]:

$$a(e^u, v) - (e^p, \nabla\cdot v) + (\rho g\beta e^T, v) = -a(u, v) + (-\rho u_h\cdot\nabla u_h - \rho g\beta(T_h - T_\infty), v) + (p_h, \nabla\cdot v) + \langle[\tau\cdot n - p_h n]_A, v\rangle_{\partial K\setminus\Gamma_i} + \langle\hat{t}, v\rangle_{\partial K\cap\Gamma_i}$$

$$(s, \nabla\cdot e^u) = (s, \nabla\cdot u_h)$$

$$d(e^T, w) = (-\rho c_p u_h\cdot\nabla T_h, w) - d(T_h, w) + \langle q_B, w\rangle_{\partial K\cap\Gamma_T} + \langle[q_h\cdot n]_A, w\rangle_{\partial k\setminus\Gamma_q}$$

The terms in parentheses on the right side represent the element residuals, a measure of the accuracy of the finite element solution inside an element. The terms in brackets are the average momentum and heat fluxes across element faces. Velocity and temperature errors are approximated with three quartic bubble functions associated to the midside nodes of the triangle. The pressure error is approximated with an appropriate bubble function. This results in small 10 by 10 systems of equations that are inexpensive to solve. The norms of the errors are computed as in the previous section.

Adaptive Remeshing

There remains one key issue to discuss: how to exploit the knowledge of the error distribution to design a better mesh.

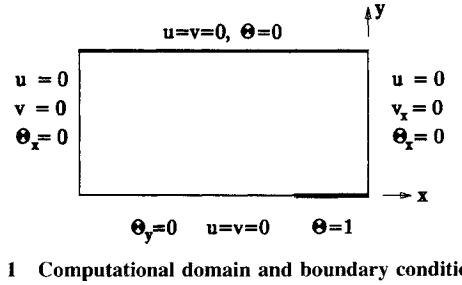

Fig. 1 Computational domain and boundary conditions.

The adaptive remeshing strategy is straightforward and follows that proposed in Refs. 1, 4, and 5, and proceeds as follows:

1 - Generate an initial mesh
2 - Compute the finite element solution
3 - Compute error estimate
4 - if (global error < tolerance) then
  - stop
  else
  - compute grid density from error estimate
  - generate an improved mesh according to grid density
  - interpolate current solution on new mesh
  - goto 2
  end if

The success of the adaptive strategy depends entirely on the adequate determination of the grid density function. It must ensure that smaller elements are generated in regions of large errors, and bigger triangles will be created where the mesh is too fine. An expression for the new element size δ may be derived from its current dimension h by invoking the principle of equidistribution of the error and combining it to the asymptotic rate of convergence of the finite element discretization. This leads to

$$\delta = \left[\frac{\eta_r\|U\|}{\|e\|\sqrt{n}}\right]^{1/k} h$$

where η_r is a target value of the relative error, n the number of elements in the mesh, and k equals 2 for the quadratic element used here. See Refs. 4, 5, and 7 for details. This distribution of element size is then used as the grid function in the advancing front mesh generator in order to generate an improved mesh.

Application

This section presents an application of the proposed adaptive remeshing methodology to the configuration studied by Chu and Hickox,[12] who considered free convection of corn syrup in an enclosure with localized heating from below.

Modeling and Boundary Conditions

The flow domain is a rectangular enclosure with a heating element of width H located at the center of the bottom wall of the cavity. Because of symmetry, only one-half of the domain is considered. Hence, the computational domain consists of a rectangle of width $2.06H$ and height $0.98H$ (see Fig. 1). The heating element is located in the lower right corner and has a dimensionless length of 0.5. Boundary conditions are shown on Fig. 1. This computational configuration is identical to that used in Ref. 12. The temperature dependence of the physical properties of corn syrup are given by[12]

$$\mu = a_0 \exp[a_1 \exp(-T/a_2)](°C, \text{poise})$$

$$a_0 = 0.2412, \quad a_1 = 12.5867, \quad a_2 = 55.7805$$

$$k = b_0 + b_1 T(°C, \text{W/mK})$$

$$b_0 = 0.3724, \quad b_1 = 3.034 \times 10^{-4}$$

$$c_p = c_0 + c_1 T + c_2 T^2(°C, \text{J/gK})$$

$$c_0 = 2.2005, \quad c_1 = 3.9532 \times 10^{-3}, \quad c_2 = -6.7883 \times 10^{-6}$$

Table 1 Parameters for the cases simulated

Case	T_0, °C	ΔT, °C	$Ra_0 \times 10^{-4}$	$Pr_0 \times 10^{-5}$	μ_0/μ_h
A	29.2	20.5	6.05	2.53	9.9
C	5.3	51.9	0.28	134.39	1026.0

Table 2 Case A, projection estimator

Mesh	No. of nodes	No. of elements	Error estimate	Solution norm
0	161	68	5.527×10^{-1}	2.121
1	327	150	3.066×10^{-1}	2.231
2	669	312	1.445×10^{-1}	2.249
3	1308	619	6.202×10^{-2}	2.249
4	2510	1203	2.579×10^{-2}	2.252
5	5243	2542	8.540×10^{-2}	2.252

Table 3 Case C, local problem

Mesh	No. of nodes	No. of elements	Error estimate	Solution norm
0	661	304	1.849×10^{-1}	2.198
1	1068	505	6.616×10^{-2}	2.191
2	2488	1199	2.960×10^{-2}	2.197
3[a]	5001	2440	1.410×10^{-2}	2.198

[a]Reduction of the error by a factor of 3.3.

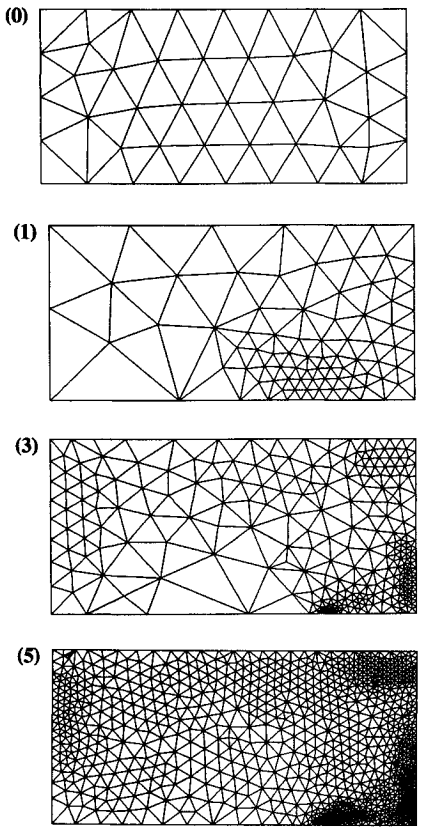

Fig. 2 Meshes for case A.

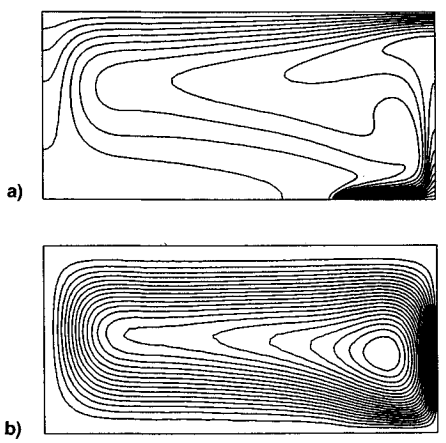

Fig. 3 Case A: temperature a) contours and b) streamlines.

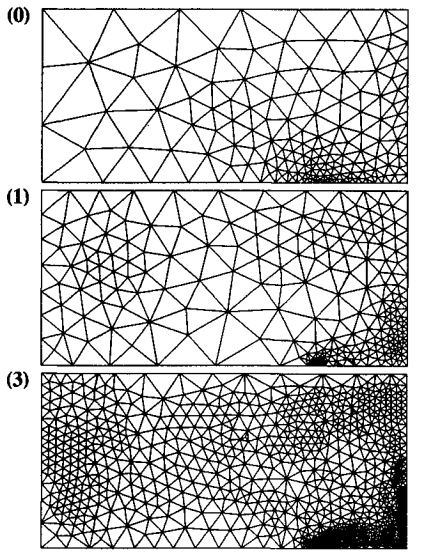

Fig. 4 Meshes for case C.

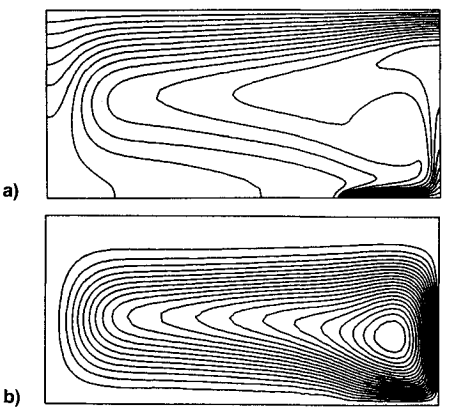

Fig. 5 Case C: temperature a) contours and b) streamlines.

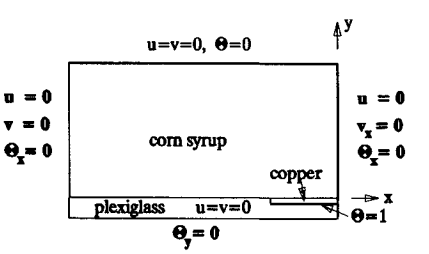

Fig. 6 Boundary conditions for the complete geometry.

Table 4 Case A, local problem

Mesh	No. of nodes	No. of elements	Error estimate	Solution norm
0	230	101	9.729×10^{-1}	2.505
1	333	156	4.747×10^{-1}	2.573
2	540	255	2.026×10^{-1}	2.540
3	966	461	1.490×10^{-1}	2.549
4	1516	733	6.477×10^{-2}	2.547
5	3356	1645	3.019×10^{-2}	2.549
6[a]	6247	3072	1.643×10^{-2}	2.549

[a]Reduction of the error by a factor of 3.

Table 5 Predicted and measured centerline velocities

Case	Plane 1, y/H, cm/min	V_1	Plane 2, y/H, cm/min	V_2
A—Measured	0.44	1.25	0.69	0.73
A—Reference 12	0.42	1.38	0.67	0.79
A—Present	0.42	1.40	0.67	0.77
C—Measured	0.40	1.68	0.65	0.88
C—Reference 12	0.39	1.92	0.64	1.05
C—Present	0.37	1.85	0.62	0.97

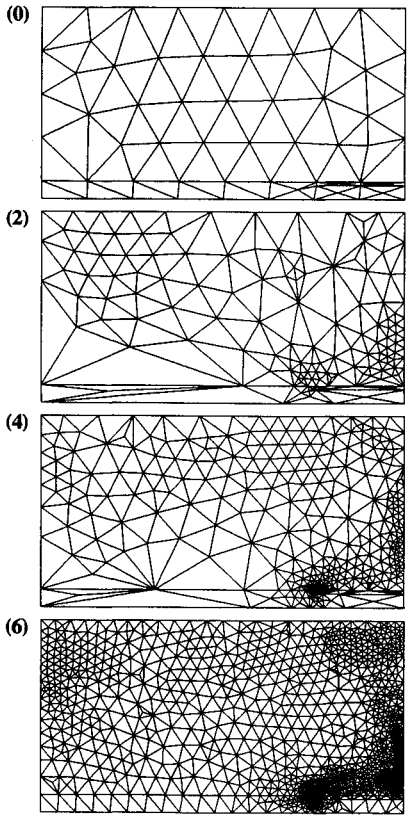

Fig. 7 Meshes for case A.

Simulations were performed for the two extreme cases considered in Ref. 12. A summary of the operating conditions is presented in Table 1.

Nondimensionalization

All calculations were performed using the following dimensionless variables:

$$x_i^* = \frac{x_i}{H}, \qquad u_i^* = \frac{u_i}{\frac{\alpha_0}{H}\sqrt{Ra_0 Pr_0}}, \qquad \theta = \frac{T - T_0}{\Delta T}$$

$$\rho^* = \sqrt{Ra_0/Pr_0}, \qquad \mu^* = \frac{\mu}{\mu_0} = f(\theta)$$

$$k^* = \frac{k}{k_0} = g(\theta), \qquad c_p^* = Pr_0 \frac{c_p}{c_{p_0}} = Pr_0 h(\theta)$$

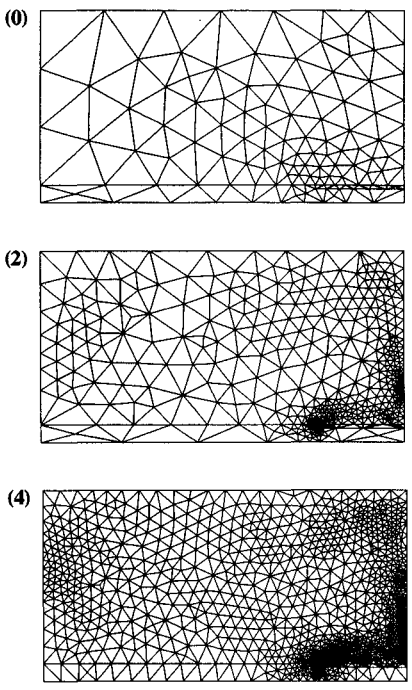

Fig. 8 Meshes for case C.

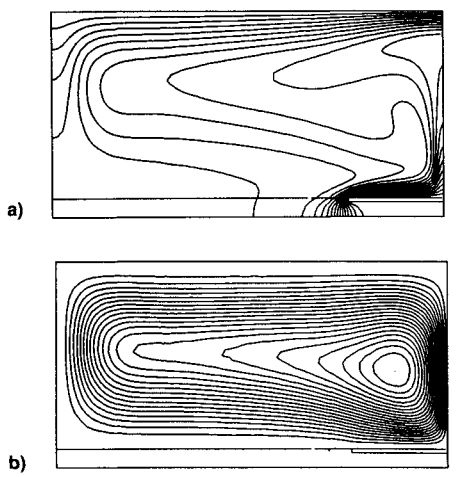

Fig. 9 Case A: temperature a) contours and b) streamlines.

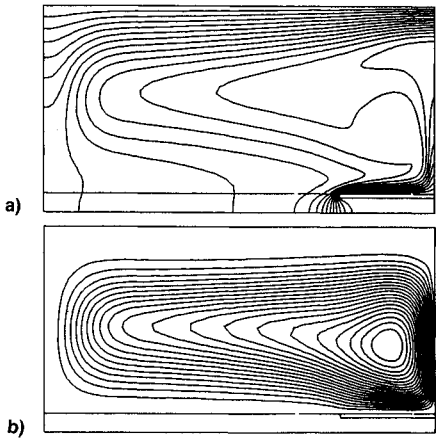

Fig. 10 Case C: temperature a) contours and b) streamlines.

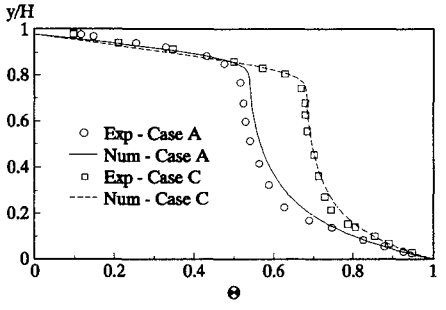

Fig. 11 Predicted and measured temperature profiles on $x = 0$.

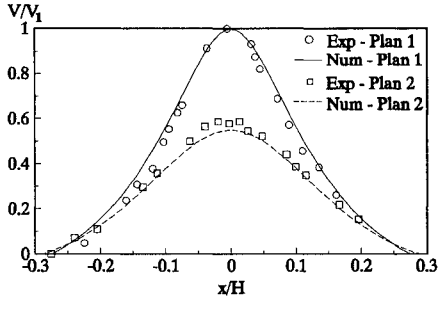

Fig. 12 Predicted and measured vertical velocity distribution for case A.

where the subscript 0 indicates that quantities are evaluated at T_0, the cold wall temperature. The Rayleigh and Prandtl numbers are defined as $Ra_0 = (g\beta\Delta TH^3)/(\nu_0\alpha_0)$, $Pr_0 = \nu_0/\alpha_0$. In these expressions $\nu_0 = \mu_0/\rho_0$ is the kinematic viscosity, and $\alpha_0 = k_0/(\rho_0 c_{p_0})$ is the thermal diffusivity.

The resulting nondimensional form of the Navier-Stokes and energy equations is

$$\sqrt{Ra_0/Pr_0}u^* \cdot \nabla u^* = -\nabla p^* + \nabla \cdot \{f(\theta)[\nabla(u^*) + \nabla(u^*)^T]\} + \sqrt{Ra_0/Pr_0}\theta$$

$$\sqrt{Ra_0/Pr_0}h(\theta)u^* \cdot \nabla\theta = \nabla \cdot [g(\theta)\nabla\theta]$$

Functions $f(\theta)$, $y(\theta)$, and $h(\theta)$ represent the temperatures dependence of μ_1, c_p, and k.

Results

The adaptive strategy was set to attempt a reduction of the error by a factor of 4 at each cycle. The codes were run in a black-box fashion requiring no user intervention. Tables 2 and 3 show the behavior of the adaptive process observed for cases A and C of Table 1. As can be seen, the rate of reduction of the error is much lower than 4. This can be explained by some of the simplifying assumptions of the computational model. Heat conduction through the thickness of the bottom wall has been neglected. This results in simple temperature boundary conditions on the bottom: a Dirichlet condition on the heating element and a zero Neumann condition on the rest of the floor (perfect insulation). This results in a singularity in the temperature gradient at the tip of the heating element, where the two boundary conditions meet. This is a severe challenge for both the flow solver and the adaptive procedure. While the singularity reduces the overall performance of the adaptive process, both error estimators still lead to improved solutions. The performance of the projection error estimator is more sensitive to the singularity. As can be seen from the tables, it predicts an increase in the error on the final mesh. This erroneous behavior is due to the projection of the heat flux that is discontinuous at the singularity.

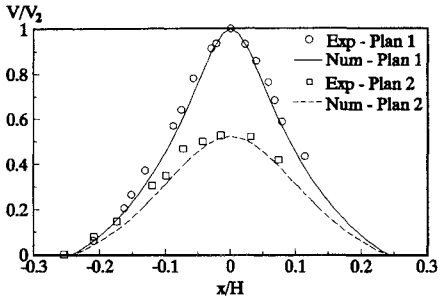

Fig. 13 Predicted and measured vertical velocity distribution for case C.

The local problem approach is more robust; Table 3 shows a monotone reduction of the error. Figure 2 shows the initial quasiuniform mesh used with both error estimators for case A. The meshes obtained at cycles 1, 3, and 5 are also presented. Similar results are produced by both methods. Hence, only one set of plots is presented. As can be seen, the adaptation produces progressive refinement near the singularity, in the plume, and near the stagnation point on the top wall. The locations of the heating element and the plume are clearly seen in the temperature contour plot of Fig. 3a. The streamlines of Fig. 3b clearly show the thinning of the boundary layer due to the decrease of the viscosity over the heating element.

Figures 4 and 5 present the same results for the more demanding case C of Ref. 12, for which the viscosity varies by more than three orders of magnitude. The flow pattern is similar, but the effects of the viscosity variation are amplified. Note that the streamlines are located much farther from the boundary in most of the domain. The top wall temperature is much lower than in case A so that the viscosity is much higher in most of the domain. The net result is that the fluid is so viscous near the solid walls that there is almost no flow in these regions. Furthermore, the temperature of the heating element is also higher for case C than for case A. This results in a much thinner boundary layer and plume.

Complete Geometry

The description of the apparatus in Ref. 12 indicates that the assumption of adiabatic lower wall may not be accurate. Hence, a simulation was performed that incorporates conduction in both the copper heating strip and in the thicker Plexiglas lower wall. This model includes horizontal and vertical conduction of heat in both solids and in the fluid. The geometry of the domain and boundary conditions are shown on Fig. 6. The bottom of the copper plate is maintained at a constant temperature. Note that in this model the heat flux is not singular at the tip of the heating element. However, the temperature gradient is still discontinuous because of the large conductivity differences between copper and Plexiglas.

Adaptation was performed using the local problem error estimator. The Dirichlet condition at the bottom of the copper element causes the heat flux to be discontinuous at this location, so that the projection technique is not very useful. Table 4 presents a summary of the adaptation process for case A.

For the simplified geometry, 6651 nodes were generated on the fifth mesh, whereas there are only 3356 for the full geometry. This is in most part due to the elimination of the singularity at the tip of the heating strip.

Figures 7 and 8 show the sequence of meshes generated by the adaptive procedure for cases A and C. The effects of viscosity variations are well reflected in the meshes for case C: thinner boundary layer and plume, and weaker stagnation point on the top wall. Figures 9 and 10 present isotherms and streamlines. While streamlines are similar for both configurations, the isotherms are very different near the bottom of the cavity. The temperature contours are not perpendicular to the wall, indicating that the adiabatic assumption was not accurate.

Figure 11 presents a comparison of predicted and measured temperature along the vertical centerline of the cavity. The conduction layer near the top wall is clearly seen. It is thicker for case C, which presents a larger viscosity contrast. Figures 12 and 13 present the distribution of vertical component of velocity along horizontal lines passing through the vortex center (plane 1), and $H/4$ above it (plane 2). In both figures the velocity is normalized by its centerline value on plane 1. While these profiles are in good agreement with the measurements, Table 5 shows that the magnitude of the predicted and measured centerline velocity differ by as much as 14%. The predictions of Ref. 12 are included in this table and show similar trends. Chu and Hickox report an uncertainty of no more than 7% in the measurements, which could explain part of the discrepancy.

The data in Table 5 and Ref. 12 indicates that this discrepancy increases with viscosity contrast. A possible origin could be the superexponential fit to the experimental measurement of viscosity, which is quoted to be accurate to 3.5%. This can result in a large uncertainty in absolute terms given the extremely large viscosity contrast.

Computational Efficiency

Results presented in the preceding section illustrate the improved resolution that can be achieved with adaptivity. The proposed adaptive strategy also results in a cost-effective solution algorithm that is well worth the added complexity.

Table 6 contains computational statistics obtained on an IBM E/S 9000 with vector facility, for case A, on the reduced geometry, using the projection estimator. Timings, in seconds, include all aspects of computations (grid generation, flow solution, error estimation, and interpolation of the solution between grids).

Computation of the error estimate represents typically less than 10% of the cost of obtaining a solution on a given mesh. Complete solution of this problem required a total of 735 CPU s. Solving the same problem directly on the final mesh without using intermediate grids would have required approximately 1550 CPU s. The computational savings are not as spectacular as those observed for constant property laminar flows, (see Ref. 5), due to the strong nonlinearities in the diffusion terms, but the adaptive strategy still proves cost-effective.

Table 6 Computational statistics for adaptation

Cycle	No. of iterations	Meshing, s	Solution, s	Adaptation, s
0	10	0.27	4.50	0.70
1	6	1.21	9.82	1.50
2	4	2.00	19.91	3.11
3	4	3.79	63.39	6.43
4	3	8.05	80.50	12.15
5	3	18.93	465.61	32.61

It should also be noted that without adaptivity it would have been nearly impossible to generate a grid leading to comparable accuracy without at least doubling the number of grid points on the final mesh. In fact, it is very difficult to achieve a good allocation of grid points without the extra knowledge gained from the error estimates. Given that Gaussian elimination is used at each Newton iteration, the increase in computational cost is proportional to the cube of the number of grid points. It follows that nonadaptive computations of comparable accuracy would have been far more expensive than adaptive ones.

Conclusions

An adaptive remeshing finite element procedure has been presented for solving problems with very large viscosity variations. The proposed adaptive procedure is very robust and can be used in a nearly black-box fashion with little or no intervention on the part of the user. Predictions for thermal convection in an enclosure with localized heating from below show good agreement with the experiments, and confirm previous computational observations.

References

[1]Peraire, J., Vahdati, M., Morgan, K., and Zienkiewicz, O. C., "Adaptive Remeshing for Compressible Flows," *Journal of Computational Physics*, Vol. 72, No. 2, 1987.

[2]Wu, J., Zhu, J. Z., Szmelter, J., and Zienkiewicz, O. C., "Error Estimation and Adaptivity in Navier-Stokes Incompressible Flows," *Computational Mechanics*, Vol. 6, No. 3, 1990, pp. 259–270.

[3]Wang, K. C., and Carey, G. F., "Adaptive Grids for Coupled Viscous Flow and Transport," *Comp. Meth., Appl., Mech. Engng.*, Vol. 82, No. 4, 1990, pp. 365–383.

[4]Hétu, J.-F., and Pelletier, D., "Adaptive Remeshing for Viscous Incompressible Flows," *AIAA Journal*, Vol. 30, No. 8, 1992, pp. 1986–1992.

[5]Hétu, J.-F., and Pelletier, D., "A Fast Adaptive Finite Element Scheme for Viscous Incompressible Flows," *AIAA Journal*, Vol. 30, No. 11, 1992, pp. 2677–2682.

[6]Pelletier, D., and Hétu, J.-F., "An Adaptive Finite Element Methodology for Incompressible Viscous Flows," Advances in Finite Elements for Fluid Dynamics II, American Society for Mechanical Engineers Winter Annual Meeting, Anaheim, CA, Nov. 1992.

[7]Pelletier, D., Hétu, J.-F., and Ilinca, F., "Adaptive Finite Element Method for Thermal Flow Problems," *AIAA Journal*, Vol. 32, No. 4, 1994, pp. 741–747.

[8]Pelletier, D., Ilinca, F., and Hétu, J.-F., "An Adaptive Finite Element Method for Turbulent Free Shear Flow Past a Propeller," AIAA Paper 93-3388, July 1993.

[9]Booker, J. R., "Thermal Convection with Strongly Temperature-Dependent Viscosity," *Journal of Fluid Mechanics*, Vol. 76, Pt. 4, 1976, pp. 741–754.

[10]Torrance, K. E., and Turcotte, D. L., "Thermal Convection with Large Viscosity Variations," *Journal of Fluid Mechanics*, Vol. 47, Pt. 1, 1971, pp. 113–125.

[11]Richter, F. M., Nataf, H.-C., and Daly, S. F., "Heat Transfer and Horizontally Averaged Temperature of Convection with Large Viscosity Variations," *Journal of Fluid Mechanics*, Vol. 129, No. 1, 1983, pp. 173–192.

[12]Chu, T. Y., and Hickox, C. E., "Thermal Convection with Large Viscosity Variation in an Enclosure with Localized Heating," *Journal of Heat Transfer*, Vol. 112, No. 3, 1990, pp. 388–395.

[13]Pelletier, D., and Fortin, A., "Are FEM Solutions of Incompressible Flows Really Incompressible? (Or How Simple Flows Can Cause Headaches)," *International Journal for Numerical Methods in Fluids*, Vol. 9, No. 1, 1989, pp. 99–112.

[14]Zienkiewicz, O. C., Gago, J. P., and Kelley, D. W., "The Hierarchical Concepts in Finite Element Analysis," *Computers and Structures*, Vol. 16, No. 1, 1983, pp. 53–65.

[15]Lohner, R., Morgan, K., and Zienkiewicz, O. C., "Adaptive

Grid Refinement for the Euler and Compressible Navier-Stokes Equations," *Accuracy Estimates and Adaptive Refinement in Finite Element Computations*, Wiley, New York, 1986.

[16]Fortin, M., and Fortin, A., "Experiments with Several Elements for Incompressible Flows," *International Journal for Numerical Methods in Fluids*, Vol. 5, No. 9, 1985, pp. 911–928.

[17]Zienkiewicz, O. C., and Zhu, R. J. Z., "A Simple Error Estimator and Adaptive Procedure for Practical Engineering Analysis," *International Journal for Numerical Methods in Engineering*, Vol. 24, 1987, pp. 337–357.

[18]Hétu, J.-F., "Méthode d'Éléments finis Adaptatives pour les Écoulements Visqueux Incompessibles," Ph.D. Dissertation, École Polytechnique de Montréal, Montréal, Québec, Canada, Dec. 1991.

[19]Oden, J. T., Demkowicz, L., Strouboulis, T., and Devloo, P., "Adaptive Methods in Solid and Fluid Mechanics," *Accuracy Estimates and Adaptive Refinement in Finite Element Computations*, Wiley, New York, 1986.

[20]Oden, J. T., "The Best FEM," *Finite Element in Analysis and Design 7*, 1990, No. 2, pp. 103–114.